Note on the time evolution sample for typeIIB PBH formation

A. Initial condition and parameter settings

Here we consider the adiabatic perturbation generated by the initial curvature perturbation ζ. As is described in Ref. [1], once the spatial profile of ζ is specified, the growing mode solution can be described up through the next-to-leading order of the long-wavelength approximation. We use the analytic expressions for the geometrical variables with the constant-mean-curvature and zero-shift gauge up through the next-to-leading order as the initial data for the sample code.

In this sample code, we consider the numerical domain given by $0 \leq R \leq L$ with R being the radial coordinate of the isotropic coordinate system. The specific profile of the initial curvature perturbation is the same as in Ref. [2][1]:

$$\zeta = -\mu \exp\left(-\frac{1}{2}k^2R^2\right) W(R), \tag{1}$$

where the function $W(R)$ is given by [4]

$$W(R; R_{\rm W}, L) = \begin{cases} 1 & \text{for } 0 \leq R \leq R_{\rm W} \\ 1 - \frac{\left((R_{\rm W}-L)^6-(L-R)^6\right)^6}{(R_{\rm W}-L)^{36}} & \text{for } R_{\rm W} \leq R \leq L \\ 0 & \text{for } L \leq R \end{cases} \tag{2}$$

with $R_{\rm W} = 0.8L$. The parameters k and μ are set as $k = 10/L$ and $\mu = 1.8$. The amplitude μ is slightly larger than the threshold value $\mu_{\rm th} \simeq 0.805$ for PBH formation reported in Ref. [3].

The background universe is assumed to be radiation-dominated, and the Hubble parameter at the initial time $H_{\rm i}$ is set to be $H_{\rm i} = 100/L$. The coordinate length L is covered by 400 grid points with grids on both ends. Since this sample code is just for demonstration, we do not seriously consider the constraint violations.

B. CARTOON method

The spherically symmetric numerical code COSMOS-S is firstly used in Ref. [5]. We perform the spherically symmetric relativistic simulation by using the CARTOON method [6]. That is, we solve the evolution equations on the Z-axis and create the necessary data around it based on the spherical symmetry with the 3rd order spline interpolation. A schematic figure for the CARTOON method is shown in Fig. 1.

[1] The functional form is slightly different from that in Ref. [3]. The difference can be absorbed into the difference in the definition of the wave number k.

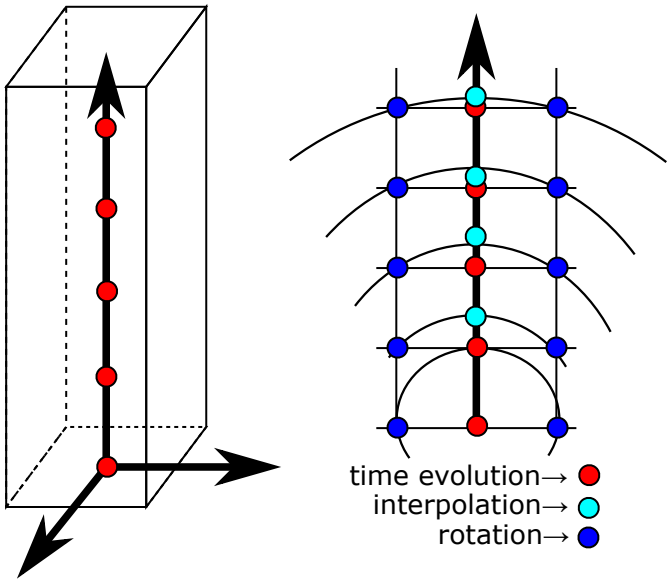

FIG. 1: A schematic figure for the CARTOON method.

C. Boundary condition

For the boundary condition, we adopt the asymptotically FLRW condition, but the constraints are significantly violated on the boundary through time evolution. The constraint violation at the boundary starts to occur when the effects of the inhomogeneity reach the boundary, and the origin of the constraint violation is due to unphysical reflected modes. As far as we know, no established procedure to reduce the unphysical reflected modes has been reported for the asymptotically FLRW boundary. Therefore the time evolution should be terminated before the boundary effects influence the dynamics of interest. We do not seriously consider this issue in this sample code. Because it is just for a demonstration. In order to avoid detecting a significant constraint violation due to the boundary effect, we exclude the outer 1/20 region from the region for checking the constraint violation. The user who wants to change the region has to change the value of the parameter exclude_boundary_rate in `cosmos_s.h`.

D. Non-Cartesian coordinate

In this sample code, we employ the non-Cartesian coordinate system (x, y, z) firstly implemented in Ref. [4]. The non-Cartesian coordinate z is related to the Cartesian coordinate Z as follows:

$$Z = z - \frac{\eta}{1+\eta}\frac{L}{\pi}\sin\left(\frac{\pi}{L}z\right). \tag{3}$$

This functional form satisfies $z = 0$ at $Z = 0$ and $z = L$ at $Z = L$. At the origin, the infinitesimal interval in the Cartesian coordinate ΔZ is covered by the non-Cartesian

coordinate interval $\Delta z = (1+\eta)\Delta Z$. Therefore the central part is enlarged in this non-Cartesian coordinate system. In this sample code, the value of η is set to 10.

E. Horizons

The trajectories of future and past trapping horizons are shown in Fig. 2. The horizon trajectories are recorded in the file `out_horizon_00.dat`. The first column is the recorded time, and the coordinate radius and the areal radius are recorded in the $2n$-th and $(2n+1)$-th columns with $n = 1, 2, \cdots$, respectively. For a sufficiently fine resolution and sufficiently small value of the parameter *horizon formation check interval* in the parameter file `par_ini.dat`, all segments of the horizon trajectories are recorded independently in different columns. But if the grid interval, or the parameter value is not sufficiently small, some of them may be regarded as one common sequence.

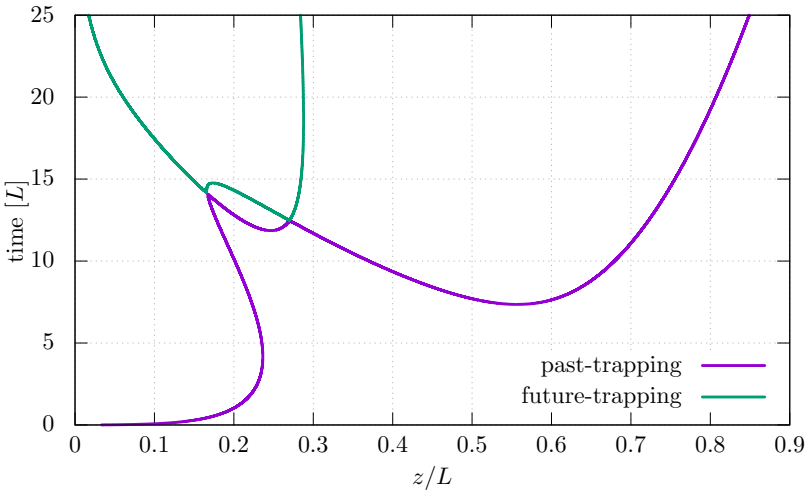

FIG. 2: Future and past trapping horizon trajectories.

[1] T. Harada, C.-M. Yoo, T. Nakama, and Y. Koga, Phys. Rev. **D91**, 084057 (2015), arXiv:1503.03934, *Cosmological long-wavelength solutions and primordial black hole formation.*

[2] K. Uehara, A. Escrivà, T. Harada, D. Saito, and C.-M. Yoo, JCAP **01**, 003 (2025), arXiv:2401.06329, *Numerical simulation of type II primordial black hole formation.*

[3] C.-M. Yoo, T. Harada, and H. Okawa, Phys. Rev. D **102**, 043526 (2020), arXiv:2004.01042, *Threshold of Primordial Black Hole Formation in Nonspherical Collapse*, [Erratum: Phys.Rev.D 107, 049901 (2023)].

[4] C.-M. Yoo, T. Ikeda, and H. Okawa, Class. Quant. Grav. **36**, 075004 (2019), arXiv:1811.00762, *Gravitational Collapse of a Massless Scalar Field in a Periodic Box.*

[5] C.-M. Yoo, T. Harada, S. Hirano, H. Okawa, and M. Sasaki, Phys. Rev. D **105**, 103538 (2022), arXiv:2112.12335, *Primordial black hole formation from massless scalar isocurvature.*

[6] M. Alcubierre *et al.*, Int. J. Mod. Phys. D **10**, 273 (2001), arXiv:gr-qc/9908012, *Symmetry without symmetry: Numerical simulation of axisymmetric systems using Cartesian grids.*